Room-temperature ferrimagnetic multiferroic BiFe$_{0.5}$Co$_{0.5}$O$_3$ thin films with giant piezoelectric response

Baizhi Gao,[1] Lingfang Lin,[1] Chen Chen,[1] Lujun Wei,[2] Ji Wang,[2] Biao Xu,[1] Chen Li,[3,4]
Jie Bian,[4] Shuai Dong,[1,*] Jun Du,[2,3,†] and Qingyu Xu[1,3,‡]

[1]*School of Physics, Southeast University, Nanjing 211189, China*
[2]*School of Physics and Collaborative Innovation Center of Advanced Microstructures, Nanjing University, Nanjing 210093, China*
[3]*National Laboratory of Solid State Microstructures, Nanjing University, Nanjing 210093, China*
[4]*College of Engineering and Applied Sciences, Nanjing University, Nanjing 210093, China*

Single-phase multiferroic materials with large polarization and magnetization at room temperature are highly desirable but still rather rare. In this study, tetragonal-like BiFe$_{0.5}$Co$_{0.5}$O$_3$ films have been synthesized and systematically characterized. For its normal state, both the highly polar structure and ferrimagnetic net magnetization are evidenced in experimental measurements at room temperature and further confirmed using first-principle calculations. Furthermore, an abnormal state driven by voltage with lattice compression along the c axis (shorter for $\sim 20\%$) is observed, rendering very rare giant piezoelectric response in multiferroics. The magnetoelectric coupling has been confirmed by the increasing saturated magnetization from 52.47 to 163.60 emu/cm^3 after the application of electric field, which is due to the spin-state transition of Co^{3+} ions.

I. INTRODUCTION

Multiferroic materials have recently attracted wide interest due to the coexistence of multiple ferro-type orderings with simultaneous mutual couplings, which have broad and important applications [1,2]. BiCoO$_3$ (BCO) is an attractive room-temperature multiferroic material (antiferromagnetic Néel temperature $T_N = 470$ K [3] and ferroelectric Curie temperature $T_C = 800$–900 K [4]) in tetragonal structure (space group $P4mm$) with an extremely large tetragonality of $c/a = 1.267$ [3]. It possesses large ferroelectric polarization of $\sim 170\,\mu$C/cm^2 theoretically [5,6]. Furthermore, the spin states of BCO can be transformed by compression from high-spin (HS) state under low pressure to low-spin (LS) state under high pressure, with a 13% volume change [4]. The spin-state transitions may also couple with light [7], which provides more tunable degrees for multiple switching in the applications.

Although it is so attractive due to the above-mentioned large polarization and spin-state transitions, there are also some defects preventing BCO from application. Only few experimental works of BCO bulk have been reported due to the difficulty in fabrication and the instability of BCO lattice [3,4]. It may only be prepared under strict conditions of high pressure of 6 GPa and high sintering temperature of 1243 K [3], because BCO is unstable and decomposes to Co$_3$O$_4$, sillenite-like Bi$_{25}$CoO$_{39}$, or Bi$_2$O$_3$ above 720 K [3]. And, the theoretically predicted ferroelectric polarization cannot be observed resulting from a low resistivity of $10^5\,\Omega$ cm [3]. Moreover, antiferromagnetism

makes the spin-state transition more difficult for magnetic detection in applications [3]. Although BCO shows a large tetragonality with ferroelectricity as an insulator in HS, it becomes paraelectric as a semiconductor in LS state by lattice compression [3–5].

Furthermore, the applied pressure can only compress the volume for LS in a compressed lattice, which cannot be recovered to HS [4]. Some previous works suggest that pressure can be substituted by electric field through its ferroelastic property, but no evidence has been provided [5,8]. To realize the electric-field manipulation, it is more suitable to fabricate BCO in thin-film geometry. But, BCO films may exhibit an initiative compression of the lattice to LS, with its ferroelectricity being destroyed [4,9].

BiFeO$_3$ (BFO) is one of the most important multiferroic materials, due to its above room-temperature antiferromagnetic and ferroelectric orderings ($T_N = 763$ K, $T_C = 1123$ K [10,11]), which has been extensively studied after the successfully epitaxial growth by pulsed laser deposition on (001) SrTiO$_3$ substrates with a large ferroelectric polarization of 60 μC/cm^2 along the [111] direction [12]. Using (001) LaAlO$_3$ (LAO) as substrates, the epitaxial growth of monoclinic tetragonal-like (T-like) BFO films can exhibit very large tetragonality of $c/a = 1.24 \sim 1.26$ [13–16], which shows enhanced polarization up to 130 μC/cm^2 [13].

Considering the similar structures of T-like BFO to BCO, the stable lattice, the large resistivity and polarization, and the different magnetic moments of Fe and Co, solid solution of BFO and BCO with large concentration of BCO might be a possible way to solve the above-mentioned impediments for BCO. In this work, we successfully prepared BiFe$_{0.5}$Co$_{0.5}$O$_3$ (BFCO) thin films with large Co concentration up to 50%, and its structure and multiferroic properties are systematically studied.

*sdong@seu.edu.cn
†jdu@nju.edu.cn
‡xuqingyu@seu.edu.cn

II. EXPERIMENTAL DETAILS

The BFCO target was prepared by a tartaric acid modified sol-gel method with bismuth nitrate, ferric nitrate, and cobalt acetate in a molar ratio of 2:1:1 [17,18]. It is noted that BFCO phase was not formed in the target with only impurity phases. BFCO thin films were fabricated on (001) LAO substrates with $Ca_{0.96}Ce_{0.04}MnO_3$ (CCMO) as buffer layers by pulsed laser deposition with a KrF excimer laser of 248-nm wavelength [19]. The CCMO buffer layers were used as bottom electrodes with low resistivity of $\sim 10^{-1}$ Ω cm, and the in-plane lattice constants were relaxed under certain thickness to a better match for the epitaxial growth of BFCO films on LAO substrates [20]. The laser energy was 1.25 J/cm^2 in a frequency of 5 Hz for CCMO and 2 Hz for BFCO. The substrate temperature was $850\,^\circ$C and oxygen pressure was 12 Pa for CCMO, and substrate temperature of $650\,^\circ$C and oxygen pressure of 2 Pa for BFCO.

The crystal structures were characterized by x-ray diffraction (XRD) with Cu Kα radiation (1.5406 Å) (Rigaku Smartlab3). The film thickness was checked by a scanning electron microscope (SEM, Zeiss Ultra 55), and the composition of films was determined by an energy-dispersive x-ray spectroscope (EDX). Raman spectra and photoluminescence emission (PL) spectra were studied by confocal Raman spectrometer (LabRAM HR UV-Visible, HORIBA Jobin Yvon) using 325-nm laser for PL and 532-nm laser for Raman measurements, respectively. The Raman configuration is as follows: Lifter D0.3, grating 600 groove/mm, hole 150 μm, and time 20 s. The surface morphology and piezoelectric properties were characterized by a scanning probe microscope (SPM, Asylum Research Cypher). The magnetic properties were measured by a superconducting quantum interference device (Quantum Design). The electrical properties were measured by a commercial ferroelectric tester (Precision Multiferroic, Radiant Technologies), with Pt as top electrodes.

The density-functional theory (DFT) calculations were performed using the projector-augmented wave (PAW) pseudopotentials as implemented in Vienna *Ab initio* Simulation Package (VASP) code [21–24]. The revised Perdew-Burke-Ernzerhof for solids function and the generalized gradient approximation plus U method were adopted to acquire more accurate description of crystalline structure and electron correlation [24,25]. According to previous works and testing of different U_{eff} [2,26,27], the on-site Coulomb $U_{\text{eff}} = U - J = 4$ eV was applied to the $3d$ orbital of Fe and Co, using the Dudarev implementation [28]. The cutoff of plane-wave basis was fixed to 550 eV and the Monkhorst-Pack k-point mesh was $8 \times 8 \times 6$ for the minimal cell and correspondingly reduced for supercell calculations. Both the lattice constants and atomic positions were fully relaxed until the force on each atom was below 0.01 eV/Å. The standard Berry-phase method was adopted to estimate the ferroelectric polarization [29].

III. RESULTS AND DISCUSSION

Figure 1 shows the XRD pattern of BFCO film. For comparison, a BFO film prepared under the same conditions is also studied, as shown in Fig. 1(a). As can be seen, only (00n) diffraction peaks can be observed for both BFCO and
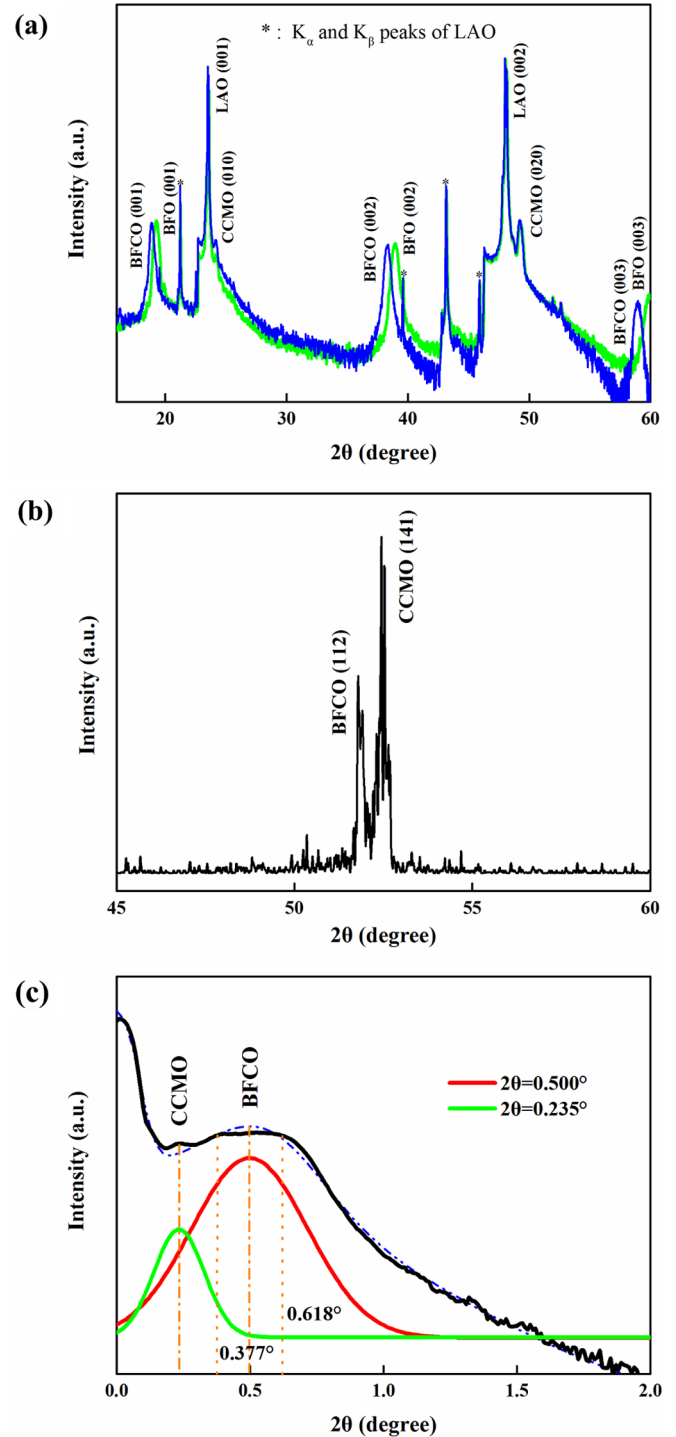
FIG. 1. (a) XRD patterns of BFCO (blue) and BFO (green) films on CCMO/LAO substrates. (b) Grazing-incidence coplanar asymmetric diffraction pattern of BFCO film. (c) Small-angle diffraction pattern of BFCO film.

BFO, indicating the pure phase and perfect (001)-oriented epitaxial growth on CCMO buffered LAO substrates. Obvious position difference between BFCO and BFO can be seen, and all the (00n) peaks of BFCO shift to smaller angles, which is in agreement with a larger c-axis lattice constant of BCO ($c = 4.723$ Å [3]) than that of T-like BFO ($c = 4.65$ Å)

[13,16]. The c-axis lattice constant calculated from XRD patterns is 4.70(2) Å for BFCO and 4.60(5) Å for BFO. The in-plane lattice constant of BFCO is measured through the grazing-incidence coplanar asymmetric diffraction method by XRD, as shown in Fig. 1(b). The diffraction peaks from BFCO and CCMO layers are shown with the peak at 52.44° from CCMO (141) and the peak at 51.93° from BFCO (112), respectively. The in-plane lattice constants are calculated to be $a = 3.74(7)$ Å for BFCO and $a = 3.76(9)$ Å for CCMO. The a-axis lattice constant for tetragonal BCO (bulks) is 3.729 Å [3], and that for T-like BFO is 3.77 Å [14], so it is expected to be ∼3.75 Å for BFCO using Vergard law. The a-axis lattice constant of CCMO is 3.73 Å [19], but the observed lattice constant of CCMO layer is a little larger. This is induced by the epitaxial strain from larger lattice constant of 3.792 Å from LAO [30,31]. Because of the incomplete relaxation of CCMO due to its small thickness, the slight expansion (comparing to 3.73 Å) of the in-plane lattice constant occurs. The lattice constant of 3.76(9) Å for CCMO is favorable for a more stable framework of BFO with its lattice constant of 3.77 Å [14], due to the previous calculation that T-like BFO is more stable when the lattice mismatch with the substrate is smaller. This has been proved by preparing pure T-like BFO film with its thickness up to 480 nm on a relaxation-controlled NdAlO$_3$ (bulk $a = 3.74(7)$ Å [32]) buffer layer on LAO substrate [20]. This further helps for the higher concentration of Co in BFO. In previous works, due to the Co-induced instability, the highest concentration of Co in BFO is only up to 30% [33–37]. In this work, we successfully fabricated BFCO films with an extremely large Co concentration up to 50%, based on the more stable BFO framework resulting from the matched lattice constants. Hence, the tetragonality c/a of BFCO is 1.25(6), which is much closer to BCO ($c/a = 1.267$ [3]) than BFO [$c/a = 1.22(0)$].

To determine the thickness of CCMO and BFCO layers, the small-angle diffraction pattern was measured and is shown in Fig. 1(c). There are obviously two peaks, one at around 0.235° and the other at 0.500°. The peak at 0.500° is quite broad, which is due to a fluctuant surface. The stronger intensity and smoother crest of the peak at 0.500° suggests its relatively outer position of the film (BFCO layer). The narrower peak at 0.235° with weaker intensity reveals its relatively inner position with smoother surface (CCMO layer). The thickness of BFCO layer is calculated about 18 nm, and the thickness of CCMO layer is about 37 nm.

The thickness of each layer was further determined by the cross-sectional SEM image, as shown in Fig. 2(a). The thickness is ∼ 20 nm for BFCO and ∼ 40 nm for CCMO, which is consistent with the values determined by XRD. The surface morphology of BFCO surface was studied by SEM, as shown in Fig. 2(b). It shows some cross-linked short lines with similar size. The surface morphology was further studied by atomic force microscopy, as shown in Fig. 2(c). The cross-linked short bar structure can be clearly observed, with surface fluctuation around 8 nm and the root-mean-square value of 2.77 nm. This indicates the three-dimensional island growth mode. The elongation of the island along one direction might be due to the relaxation of the lattice constants. However, due to the cubic in-plane lattice for CCMO, the relaxation along
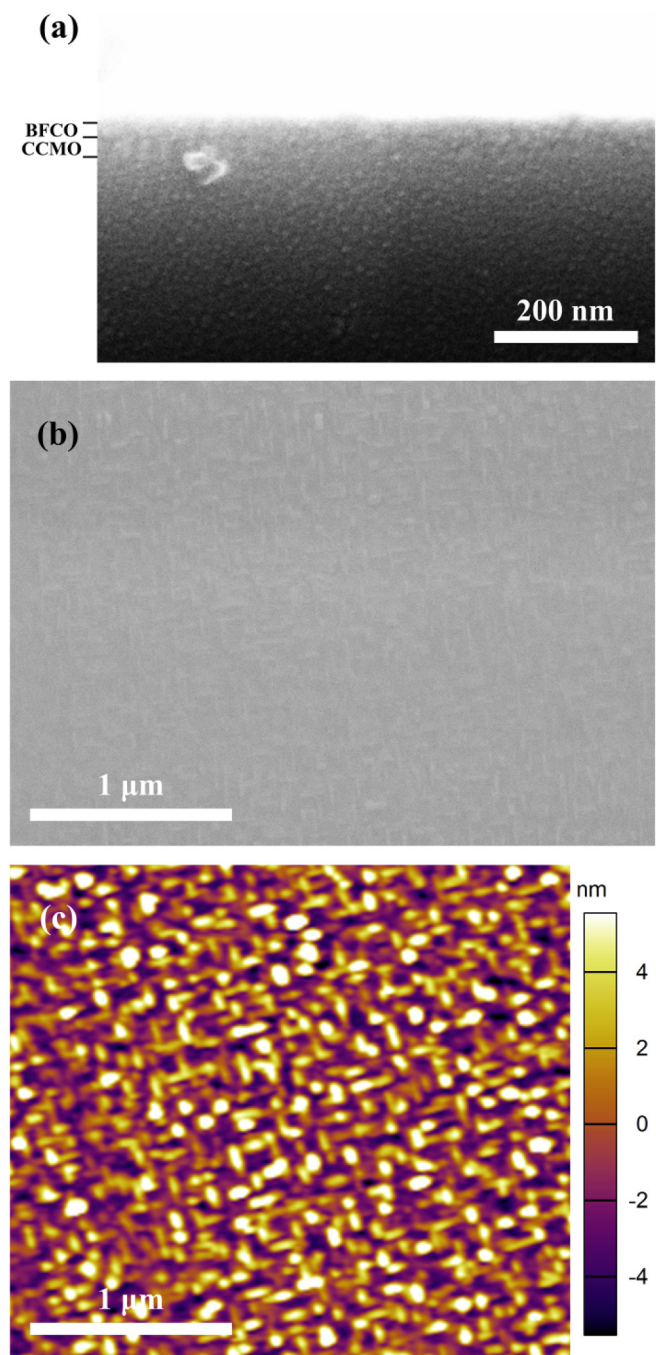
FIG. 2. (a) Cross-sectional and (b) plane-view images of BFCO films by SEM. (c) Surface morphology of BFCO film by atomic force microscopy.

the two orthogonal directions are nearly equivalent. The exact concentration of each element in the film was studied by EDX, and results are listed in Table I. It can be clearly seen that Co and Fe have equal concentration in BFCO.

The structure of the BFCO films was further studied by Raman and PL spectra, as shown in Fig. 3. The CCMO/LAO substrate has also been studied (see Fig. S1 in Supplemental Material [38]) and the deducted Raman spectrum for BFCO layer is shown in Fig. 3(a). It has been reported that the epitaxial BFO on LAO substrate is actually monoclinic T-like structure

TABLE I. Measured concentrations of each element in BFCO film by EDX.

Elements	La	Al	Ca	Mn	Bi	Fe	Co
Layers		$LaAlO_3$		$Ca_{0.96}Ce_{0.04}MnO_3$		$BiFe_{0.5}Co_{0.5}O_3$	
Wt. %	61.4	11.1	0.9	1.3	5.0	0.6	0.6
At. %	46.6	43.3	2.4	2.5	2.5	1.1	1.1

(space group *Cc*) rather than tetragonal structure (*P4mm*) [14,39,40]. Theoretically, there are only four ($3A_1 + B_1$) Raman lines in the case of tetragonal BFO, but many more lines are observed, with peaks at 146, 227, 273, 587, and 691 cm^{-1} for A' modes and peaks at 220, 242, 266, and 368 for A'' modes, revealing its *T*-like structure [15]. Thus, it can be clearly distinguished between tetragonal and *T*-like structures based on the number of peaks. Note that thin films can have lattice mismatch with the substrate, which induces thickness-dependent lattice constant gradients. However, the mismatch between LAO and CCMO is much larger than that between CCMO and BFCO. Therefore, it is reasonable to consider that there is no new mode introduced by depositing BFCO on CCMO. The thickness of BFCO is only about 20 nm, which is very thin, and it can be considered that the lattice constant of BFCO fully matches that of CCMO. Hence, there would

be no peak related to lattice mismatch in the deducted Raman spectrum for BFCO layer. Although there is no report on the Raman spectra of BCO and BFCO, similar Raman spectra to that from *T*-like BFO can be expected in BFCO films. Several modes at 147.3, 220.5, 243.2, 269.7, and 369.8 cm^{-1} can be resolved as shown in Fig. 3(a), which can be assigned to the *T*-like BFCO by comparing with the A' and A'' modes of *T*-like BFO [15]. This is consistent with the theoretical calculated crystalline structure for BFCO [41]. The slight violet shift of Raman modes in BFCO comparing to those of *T*-like BFO is due to the relatively larger mass of Co comparing to Fe. The peaks at larger Raman shift can hardly be distinguished due to the noise.

PL spectrum is considered as a suitable method to determine the band gaps of materials in thin-film geometry [42–44]. Hence, the band gap of BFCO film is determined, as shown in Fig. 3(b). The PL spectrum of CCMO/LAO substrate has been subtracted [19]. Three main peaks can be clearly resolved, locating at 496.3, 526.2, and 561.3 nm, respectively. The previous works reported that the band gap of *T*-like BFO is around $E_g = 3.10$ eV [45], and BCO theoretically around $E_g = 2.11$ eV [46,47]. The strongest peak at 496.3 nm indicates the main energy gap of $E_g = 2.50$ eV, while the other lower ones are at 2.36 and 2.22 eV, respectively. It is reasonable to consider the narrow and strong peak at $E_g = 2.50$ eV as the main band gap of BFCO film [44]. The two lower peaks might be due to some local defect states.

The in-plane and out-of-plane magnetizations of BFCO were both measured, which are shown in Fig. 4. To derive the magnetic properties of BFCO layer, a CCMO layer was deposited on LAO substrate under the same conditions, and measured in the same way. The linear backgrounds of both hysteresis loops are subtracted, as shown in Figs. 4(a)–4(d). By subtracting the magnetic background of CCMO, the magnetic hysteresis loops of BFCO film are shown in Figs. 4(e) and 4(f), demonstrating the weak ferromagnetism at 5 K. They exhibit a larger out-of-plane saturated magnetization of 52.47 emu/cm^3 than in-plane value of 18.95 emu/cm^3. At 300 K, saturated magnetizations are 22.37 emu/cm^3 in the out-of-plane direction and 7.05 emu/cm^3 in the in-plane direction. Thus, BFCO shows a remarkable magnetic anisotropy, which suggests that the magnetic moment prefers to be aligned along the *c* axis. It is reasonable that the magnetic anisotropy is usually observed in tetragonal structured materials, because of their anisotropy in lattice symmetry and the large displacement of O from octahedron to pyramid geometry [48–50]. The appearance of magnetic anisotropy in BFCO is expected; the same preference of magnetic moment direction (along the *c* axis) has been observed in BCO bulks [3]. In Figs. 4(a)–4(d), the insets exhibit the magnified views of the small-field regions. We can obviously see the enlarged coercive fields of BFCO/CCMO comparing to CCMO background. The coercivities of CCMO are
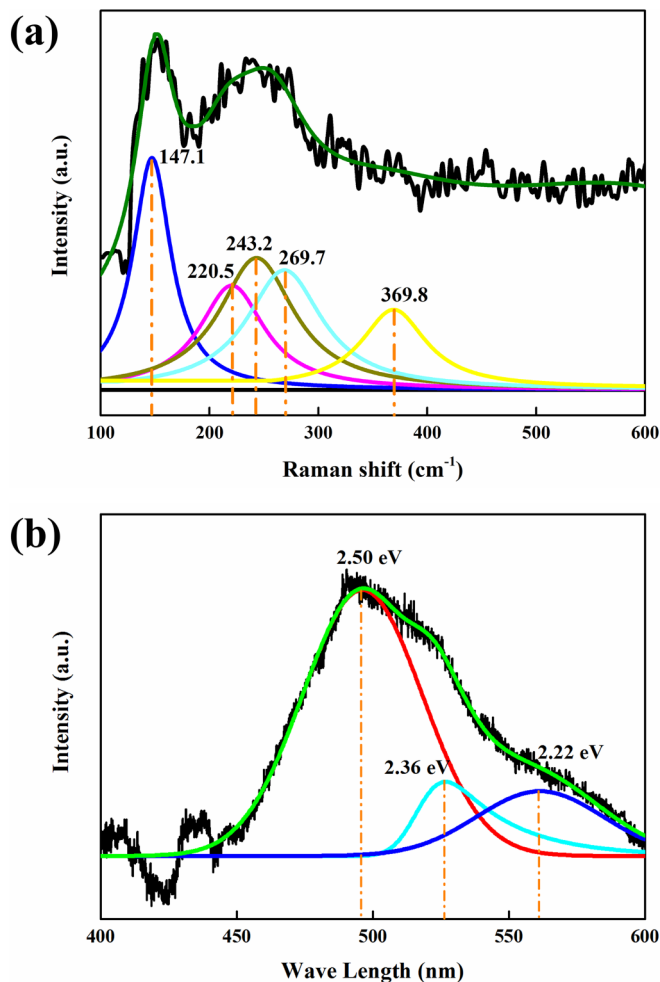
FIG. 3. (a) Raman spectrum and (b) PL spectrum of BFCO film.
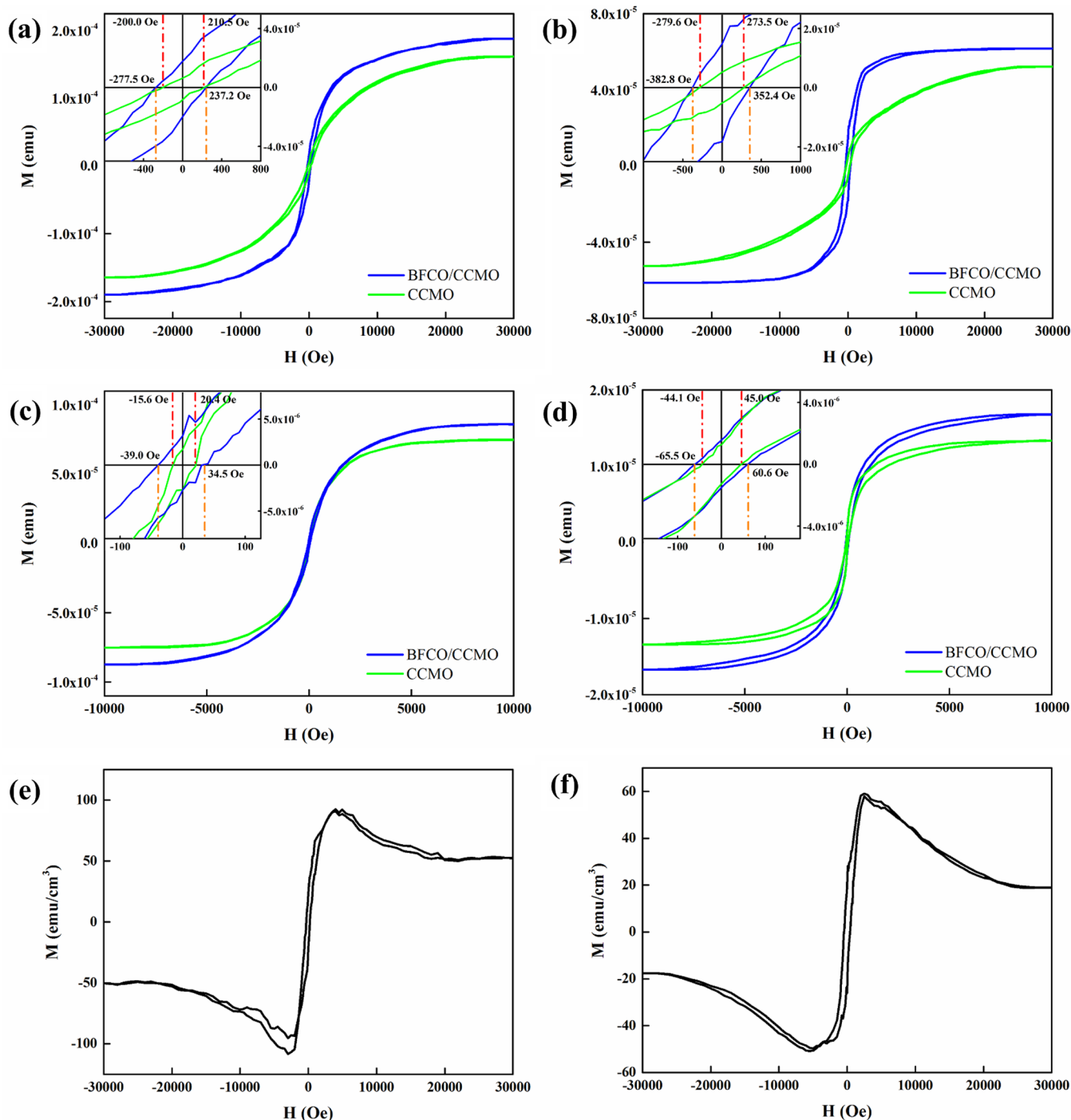
FIG. 4. Magnetic hysteresis loops of BFCO/CCMO and CCMO films with field in out-of-plane direction (a) (5 K) and (c) (300 K), and in-plane direction (b) (5 K) and (d) (300 K). (e), (f) Deducted magnetic hysteresis loops of BFCO with field in out-of-plane and in-plane directions at 5 K, respectively. The insets are the magnified views of small-field regions, with coercivities of BFCO/CCMO (orange) and CCMO (red) marked by dashed lines, respectively.

nearly symmetric to zero field. However, the magnetic hysteresis loops of BFCO/CCMO all obviously shift to negative fields, indicating the exchange bias. The abnormal shapes of magnetic hysteresis loops for BFCO in Figs. 4(e) and 4(f) might be due to the exchange coupling between BFCO and CCMO layer.

For better understanding of the magnetic ordering and net magnetization in BFCO, DFT calculations were performed. Because of the Co-induced instability in BFCO (no BCO

film has been reported), Co-enriched area ($>50\%$) can lead to impurity phases due to its decomposition, however absent in the XRD pattern. Considering the equal concentration of Fe and Co as measured in EDX, the uniform distribution of Fe and Co ions in BFCO films is expected. Hence, we only consider the well-distributed configurations. The calculated spin arrangements of Fe and Co ions are shown in Fig. 5. The most possible relevant collinear orders of Fe and Co
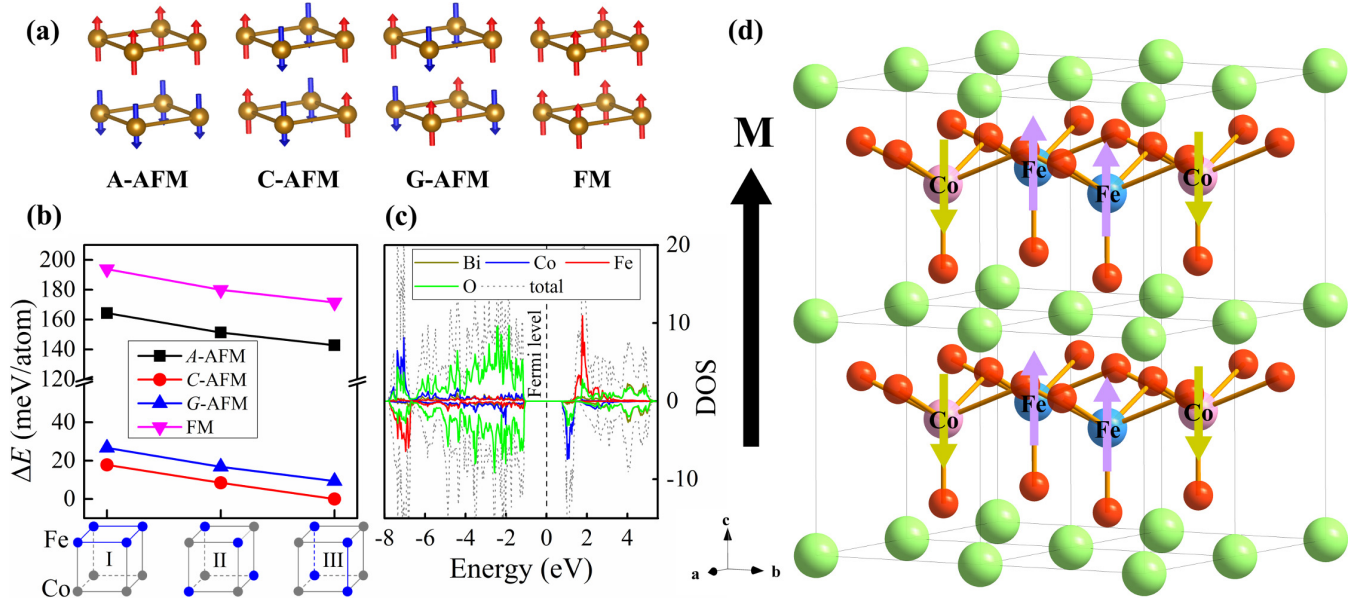
FIG. 5. (a) The considered four types of spin configurations. (b) Energies of BFCO in different magnetic orderings and Fe, Co arrangements (marked by I, II, and III) at the bottom with blue balls for Fe and gray balls for Co (*C*-AFM with type-III arrangement is taken as reference). (c) DOS and atom-projected DOS of the ground configuration. (d) Scheme of lattice and spin for *C*-FiM ordered BFCO with a net magnetic moment.

spins are considered, including *A*-type antiferromagnetic (*A*-AFM), *C*-type antiferromagnetic (*C*-AFM), *G*-type antiferromagnetic (*G*-AFM), and ferromagnetic (FM) orderings, shown in Fig. 5(a) [51]. According to the crystal symmetry, three different arrangements of magnetic atoms labeled as I, II, III of BFCO are considered as shown in Fig. 5(b). The calculated energies clearly show that *C*-AFM ordering is always the most stable structure and the type-III arrangement is always the most stable configuration. Similar result of C-AFM spin ordering as the ground state for BFCO has been recently reported [52]. According to the considered combination of magnetic orderings and atom arrangements, there are only three configurations that can exhibit a net magnetization in BFCO, which are *C*-AFM with type-III arrangement (*C*-FiM), *G*-AFM with type-II arrangement (*G*-FiM), and *A*-AFM with type-I arrangement (*A*-FiM). The *C*-FiM ordering is the ground state, the energy of which is much lower than *G*-FiM and *A*-FiM. For comparison, the calculated data are summarized in Table II, which illustrates the quite close calculated lattice constants of *C*-FiM to our experimental ones. Furthermore, the net magnetization is calculated to be $0.5 \mu_B$/atom (i.e., ~ 70 emu/cm^3), which is in good agreement with measured maximum magnetization of 52.47 emu/cm^3 at 5 K. Hence, the most possible magnetic configuration of BFCO is *C*-FiM arrangement as shown in Fig. 5(d), and density of states (DOS) of BFCO [Fig. 5(c)] shows that it is an insulator with a band gap of 2.0 eV as we measured.

In order to change the spin states of Co in BCO bulks, high pressure was applied to compress the crystal, which led to a large volume change up to 13% [4]. It has been suggested that the pressure might be substituted for better application by electric field through its piezoelectric response [5,6,8], but no evidence has been reported for the existence of such an electric-induced large volume change and whether it is stable

and recoverable. It has been reported that Co-substituted BFO may lead to an enhancement of piezoelectric performances from BFO [53]. Compared with BFO, BFCO might provide a much larger electric-induced volume change due to the high Co concentration. In Fig. 6(a), we can see the clear amplitude and phase hysteresis loops with a maximum bias of 15 V, confirming the ferroelectric nature at room temperature. From the amplitude curve, an extremely large amplitude of ~ 1 nm can be seen. Considering the measured total thickness of 20 nm, it means that there is an $\sim 5\%$ volume change along the *c* axis. And, more amplitude and phase hysteresis loops of different points can be seen in Fig. S2 [38], which reveal the similar volume change. With such a large enough compression, BCO might exhibit spin-state transitions as reported in some theoretical works [5,54]. More importantly, the large volume change by a 15-V dc bias is recoverable and stable as shown in Fig. 6(a) and Fig. S2 [38]. With adding a dc bias voltage up to 30 V, a drastic compression appears on the surface

TABLE II. Optimized structural parameters *c* of a unit cell with experimentally fixed *ab* plane (3.747 Å), local magnetic moment of M_{Fe} for Fe and M_{Co} for Co within the default PAW sphere, and net magnetization *M* for various magnetic structures with type-III atom arrangement. The experimental values obtained from this work are also listed for comparison.

Types	c (Å)	M_{Fe}/M_{Co} (μ_B)	M (μ_B/atom)
A-AFM	4.68	4.17/3.07	0.0
C-FiM	4.64	4.08/2.98	0.5
G-AFM	4.62	4.09/2.99	0.0
FM	4.71	4.19/3.08	4.5
Experimental	4.70(2)		0.38
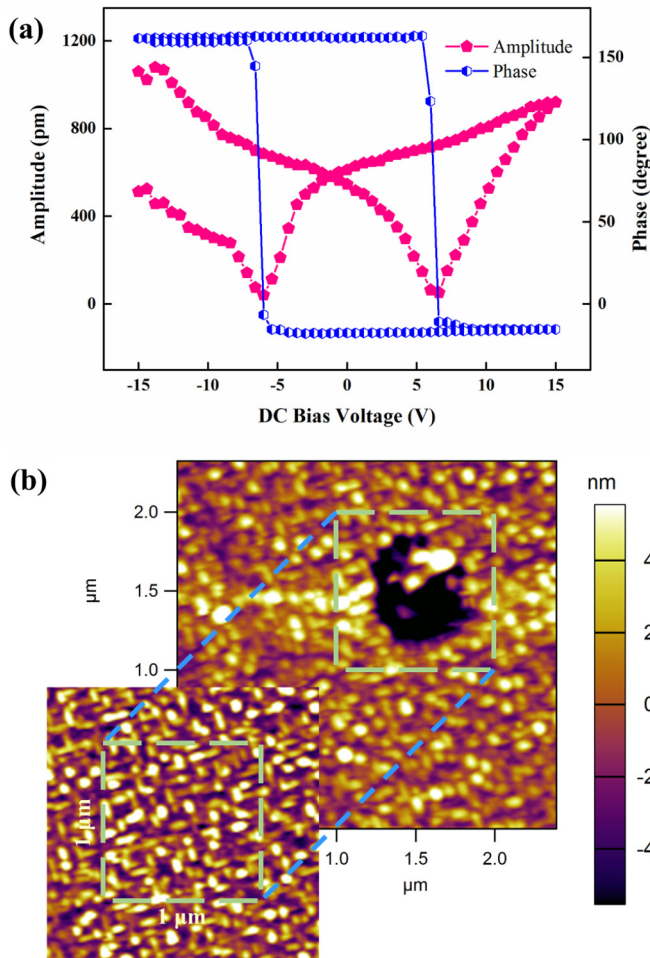
FIG. 6. (a) Phase and amplitude curves for BFCO. (b) Surface morphologies before (bottom left) and after applying a 30-V dc bias.

FIG. 7. (a) Resistivities under maximum electric field of 3.75, 5.00, and 6.25 MV/cm, before and after the application of a 25-V dc voltage for 5 min. (b) Intrinsic remanent polarization hysteresis loop of compressed BFCO.

of BFCO film, as shown in Fig. 6(b). The surface height decreases ~ 4 nm, which is $\sim 20\%$ of the total thickness of 20 nm. Considering the c-axis lattice constant of BFCO, a 20% compression would lead to a decrease from 4.70(2) to 3.76(2) Å, which suggests a large volume change from T-like to nearly cubic structure. This is similar to the results of BCO that structures transform from tetragonal to nearly cubic, with the spin state transiting from HS to LS [4,8,47].

Since electric field can perform a large volume change, we try to prepare the compression state of BFCO. A long-term applied field might drive the lattice to the new stable state, which might be finally stabilized. Through adding a 6.25-MV/cm dc electric field (25 V in voltage) for 5 min by a probe onto the top electrodes, we successfully prepared the compression state. Although the structure and spin-state characterizations are hard to carry out in such an electrode-sized region of $\sim 120\,\mu$m in diameter, resistivity might be expected to change in a similar way to BCO. The resistivity change of BFCO is demonstrated, as shown in Fig. 7(a). The resistivity is over $10^{10}\,\Omega$ cm, exhibiting a good insulating nature, which is much larger than that of BCO of $\sim 10^5\,\Omega$ cm [3,4]. This is due to BFO framework, which is a good insulator. After adding the voltage, the resistivities drastically decrease over one order of magnitude, and finally about three orders of

magnitude at 6.25 MV/cm. Such a drastic decrease of $\sim 10^3$ is due to the compression of c-axis lattice constant, which is similar to BCO that the tetragonality is compressed along with the drastic decrease of resistivity after the applied pressure [4]. And, the $\sim 10^3$ decrease of resistivity might lead to the spin-state transition [4].

As in Fig. 7(b), we measured the intrinsic remanent polarization of compressed BFCO at room temperature under various electric field, by a recently reported method of a train of 14 voltage pulses [55]. The method is explained in Fig. S3 [38]. Although BCO is reported to be paraelectric in compressed LS [4], ferroelectricity is preserved with a small intrinsic remanent polarization of $0.44\,\mu$C/cm^2 and coercivity of ~ 3.25 MV/cm in compressed BFCO. Thus, the room-temperature ferroelectricity is confirmed in compression state of BFCO. Based on the structure revealed above, our calculation of the ferroelectric polarization of BFCO in normal state (along the c axis) gives 119 and $120\,\mu$C/cm^2 using the intuitive point-charge model and standard Berry-phase method, respectively [29]. However, we did not observe any hysteresis loops in normal state of BFCO up to 7.5 MV/cm (a higher electric field than 7.5 MV/cm, namely 30 V in
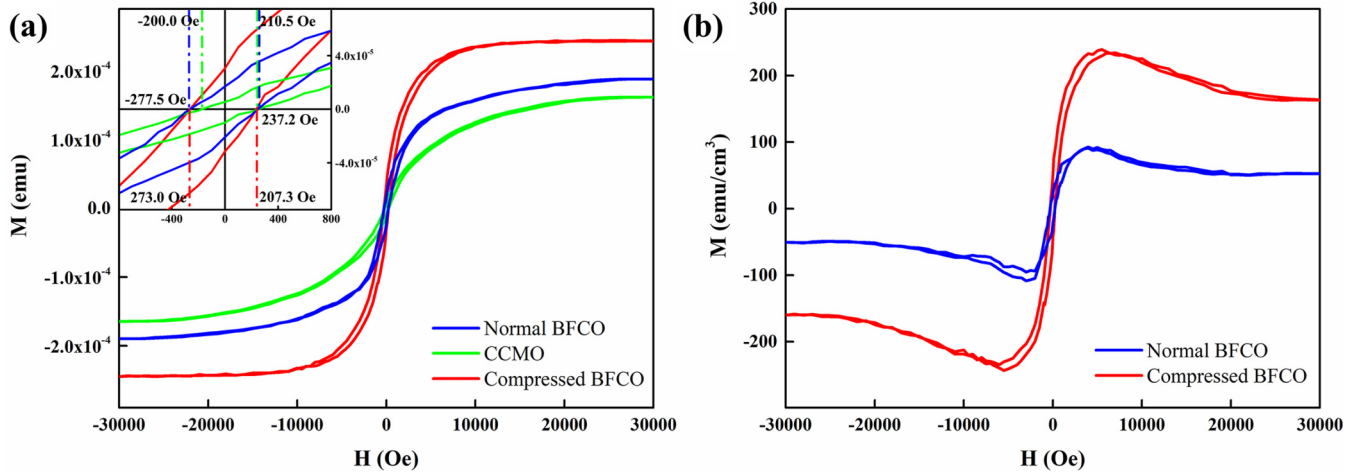
FIG. 8. (a) Magnetic hysteresis loops of normal BFCO/CCMO, CCMO, and the compressed BFCO/CCMO in out-of-plane direction at 5 K. (b) Magnetic hysteresis loops of normal BFCO and compressed BFCO films. The inset is the magnified view of small-field region, with coercivities of normal BFCO/CCMO (blue), CCMO (green), and compressed BFCO/CCMO (red), marked by dashed lines, respectively.

voltage, is confusing because we cannot distinguish whether it is from normal state or compression state or even a part from the one and a part from the other). It might be due to the competition between polarization reversal and lattice compression, since a highly polar structure requires a large electric field for reversal. The reversal voltage might be larger than that of what the compression needs, which would lead to the lattice compression preferentially.

We further characterize the magnetic switching in the compressed BFCO films with top Pt electrode after the application of 25-V dc voltage. The magnetization of the compressed BFCO film is drastically enhanced compared with BFCO in normal state, as shown in Fig. 8(a). The deducted hysteresis loops are shown in Fig. 8(b). The saturated magnetization increases from 52.47 to 163.60 emu/cm^3, which is almost 1.17 μ_B/atom for the compressed BFCO. This can be attributed to the spin-state transitions of Co from HS to LS in compression state of BFCO. It has been reported that BFO can also perform spin-state transitions (LS, $S = 1/2$) [56], and the spin-state transitions of Fe and Co are both due to the competition of crystal-field splitting and intra-atomic exchange coupling [47,54,56]. However, Fe in BFCO seems to remain its HS with the decreases of lattice constant. This can be explained by that Fe is much harder to perform spin-state transitions, since it transforms under a more extreme condition of over 40 GPa at room temperature than BCO [56]. As a result, with the lattice compression, Co mainly transforms from HS to LS and Fe prefers to maintain its spin state. The magnified view in Fig. 8(a) denotes the existence of exchange bias in compressed BFCO at 5 K.

Our results present the similar changes in tetragonality, resistivity, polarization, and magnetization of BFCO to BCO (from HS to LS state). They can be attributed to the Co spin-state transitions from BFCO in normal state to compression state. Furthermore, the recent works show that spin state of Co prefers to be mixed states of HS and LS, rather than a sudden simultaneous spin-state transition during the compression process, both experimentally and theoretically [4,57]. That means a smaller volume change, for example of ∼ 5%, has chances to exhibit an obvious change of net magnetization

in BFCO due to the mixed spin states by compression. Thus, it provides an important route for magnetoelectric coupling.

IV. CONCLUSION

In conclusion, we successfully fabricated room-temperature multiferroic BFCO films on (001) LAO substrates with CCMO conductive buffer layers. The BFCO film has T-like structure with tetragonality of $c/a = 1.25(6)$. PL spectrum suggests the band gap of 2.50 eV. It reveals a room-temperature exchange bias coupled with CCMO layer, and out-of-plane magnetic anisotropy with maximum magnetization of 52.47 emu/cm^3 along the c axis. The most possible magnetic configuration is C-FiM, based on the DFT calculations and experimental results. The volume switching by electric field is confirmed and demonstrated with a recoverable and stable volume change of ∼ 5% along the c axis under maximum voltage of 15 V by SPM. A ∼ 20% compression along the c axis under voltage of 30 V was observed, consistent with the transformation from T-like structure to nearly cubic structure, along with the drastic decrease of the resistivity from 10^{10} to 10^7 Ω cm. It renders the extremely rare giant piezoelectric response. The ferroelectricity is preserved in compressed BFCO with a small intrinsic remanent polarization of 0.44 μC/cm^2. Magnetoelectric coupling is confirmed by the drastic increase of saturated magnetization from 52.47 emu/cm^3 for normal BFCO to 163.60 emu/cm^3 for compressed BFCO under application of 25-V voltage.

[1] S. Dong, J. M. Liu, S. W. Cheong, and Z. F. Ren, Adv. Phys. **64**, 519 (2015).

[2] Y. Weng, L. Lin, E. Dagotto, and S. Dong, Phys. Rev. Lett. **117**, 037601 (2016).

[3] A. A. Belik, S. Iikubo, K. Kodama, N. Igawa, S. Shamoto, S. Niitaka, M. Azuma, Y. Shimakawa, M. Takano, F. Izumi, and E. T. Muromachi, Chem. Mater. **18**, 798 (2006).

[4] K. Oka, M. Azuma, W. Chen, H. Yusa, A. A. Belik, E. T. Muromachi, M. Mizumaki, N. Ishimatsu, N. Hiraoka, M. Tsujimoto, M. G. Tucker, J. P. Attfield, and Y. Shimakawa, J. Am. Chem. Soc. **132**, 9438 (2010).

[5] P. Ravindran, R. Vidya, O. Eriksson, and H. Fjellvag, Adv. Mater. **20**, 1353 (2008).

[6] Y. Uratani, T. Shishidou, F. Ishii, and T. Oguchi, Jpn. J. Appl. Phys. **44**, 7130 (2005).

[7] E. V. Mostovshchikova, N. N. Loshkareva, S. V. Naumov, V. A. Khokhlov, A. Yu. Prokhorov, A. V. Pashchenko, and A. S. Korneevetc, Appl. Phys. A **120**, 239 (2015).

[8] L. Weston, X. Y. Cui, S. P. Ringer, and C. Stampfl, Phys. Rev. B **93**, 165210 (2016).

[9] T. Das and T. S. Dasgupta, Dalton Trans. **44**, 10882 (2015).

[10] G. A. Smolenskii and I. Chupis, Sov. Phys. Usp. **25**, 475 (1982).

[11] C. Ederer and N. A. Spaldin, Phys. Rev. Lett. **95**, 257601 (2005).

[12] J. Wang, J. B. Neaton, H. Zheng, V. Nagarajan, S. B. Ogale, B. Liu, D. Viehland, V. Vaithyanathan, D. G. Schlom, U. V. Waghmare, N. A. Spaldin, K. M. Rabe, M. Wuttig, and R. Ramesh, Science **299**, 1719 (2003).

[13] J. X. Zhang, Q. He, M. Trassin, W. Luo, D. Yi, M. D. Rossell, P. Yu, L. You, C. H. Wang, C. Y. Kuo, J. T. Heron, Z. Hu, R. J. Zeches, H. J. Lin, A. Tanaka, C. T. Chen, L. H. Tjeng, Y. H. Chu, and R. Ramesh, Phys. Rev. Lett. **107**, 147602 (2011).

[14] H. Bea, B. Dupe, S. Fusil, R. Mattana, E. Jacquet, B. Warot-Fonrose, F. Wilhelm, A. Rogalev, S. Petit, V. Cros, A. Anane, F. Petroff, K. Bouzehouane, G. Geneste, B. Dkhil, S. Lisenkov, I. Ponomareva, L. Bellaiche, M. Bibes, and A. Barthelemy, Phys. Rev. Lett. **102**, 217603 (2009).

[15] M. N. Iliev, M. V. Abrashev, D. Mazumdar, V. Shelke, and A. Gupta, Phys. Rev. B **82**, 014107 (2010).

[16] D. Mazumdar, V. Shelke, M. Iliev, S. Jesse, A. Kumar, S. V. Kalinin, A. P. Baddorf, and A. Gupta, Nano Lett. **10**, 2555 (2010).

[17] S. Ghosh, S. Dasgupta, A. Sen, and H. S. Maiti, J. Am. Ceram. Soc. **88**, 1349 (2005).

[18] Q. Xu, X. Zheng, Z. Wen, Y. Yang, D. Wu, and M. Xu, Solid State Commun. **151**, 624 (2011).

[19] H. Yamada, M. Marinova, P. Altuntas, A. Crassous, L. B. Lours, S. Fusil, E. Jacquet, V. Garcia, K. Bouzehouane, A. Gloter, J. E. Villegas, A. Barthelemy, and M. Bibes, Sci. Rep. **3**, 2834 (2013).

[20] Q. Xu, X. Yuan, X. Xue, Z. Shi, Z. Wen, and J. Du, Phys. Status Solidi B **251**, 892 (2014).

[21] G. Kresse and J. Hafner, Phys. Rev. B **47**, 558 (1993).

[22] G. Kresse and J. Furthmuller, Phys. Rev. B **54**, 11169 (1996).

[23] G. Kresse and D. Joubert, Phys. Rev. B **59**, 1758 (1999).

[24] J. P. Perdew, K. Burke, and M. Ernzerhof, Phys. Rev. Lett. **77**, 3865 (1996).

[25] J. P. Perdew, A. Ruzsinszky, G. I. Csonka, O. A. Vydrov, G. E. Scuseria, L. A. Constantin, X. Zhou, and K. Burke, Phys. Rev. Lett. **100**, 136406 (2008).

[26] H. M. Zhang, Y. K. Weng, X. Y. Yao, and S. Dong, Phys. Rev. B **91**, 195145 (2015).

[27] M. F. Liu, L. L. Lin, Y. Zhang, S. Z. Li, Q. Z. Huang, V. O. Garlea, T. Zou, Y. L. Xie, Y. Wang, C. L. Lu, L. Yang, Z. B. Yan, X. Z. Wang, S. Dong, and J. M. Liu, Phys. Rev. B **95**, 195134 (2017).

[28] S. L. Dudarev, G. A. Botton, S. Y. Savrasov, C. J. Humphreys, and A. P. Sutton, Phys. Rev. B **57**, 1505 (1998).

[29] R. Resta, Rev. Mod. Phys. **66**, 899 (1994).

[30] H. M. O'Bryan, P. K. Gallagher, G. W. Berkstresser, and C. D. Brandle, J. Mater. Res. **5**, 183 (1990).

[31] L. P. Guo, Y. J. Tian, J. Z. Liu, S. F. Xu, L. Li, Z. X. Zhao, Z. H. Chen, D. F. Cui, H. B. Lu, Y. L. Zhou, and G. Z. Yang, Appl. Phys. Lett. **66**, 3356 (1995).

[32] C. S. Woo, J. H. Lee, K. Chu, B. K. Jang, Y. B. Kim, T. Y. Koo, P. Yang, Y. Qi, Z. Chen, L. Chen, H. C. Choi, J. H. Shim, and C. H. Yang, Phys. Rev. B **86**, 054417 (2012).

[33] S. Yasui, M. Nakajima, H. Naganuma, S. Okamura, K. Nishida, T. Yamamoto, T. Iijima, M. Azuma, H. Morioka, K. Saito, M. Ishikawa, T. Yamada, and H. Funakubo, J. Appl. Phys. **105**, 061620 (2009).

[34] L. Peng, H. Deng, J. Tian, Q. Ren, C. Peng, Z. Huang, P. Yang, and J. Chua, Appl. Surf. Sci. **268**, 146 (2013).

[35] H. Shima, K. Nishida, T. Yamamoto, T. Tadokoro, K. Tsutsumi, M. Suzuki, and H. Naganuma, J. Appl. Phys. **113**, 17A914 (2013).

[36] L. Yin, W. Mi, and X. Wang, Sci. Rep. **6**, 20591 (2016).

[37] N. T. Tho, T. Kanashima, M. Sohgawa, D. Ricinschi, M. Noda, and M. Okuyama, Jpn. J. Appl. Phys. **49**, 09MB05 (2010).

[38] See Supplemental Material at http://link.aps.org/supplemental/10.1103/PhysRevMaterials.2.084401 for more Raman spectra of samples, more phase and amplitude curves, and more details of polarization measurements.

[39] R. J. Zeches, M. D. Rossell, J. X. Zhang, A. J. Hatt, Q. He, C. H. Yang, A. Kumar, C. H. Wang, A. Melville, C. Adamo, G. Sheng, Y. H. Chu, J. F. Ihlefeld, R. Erni, C. Ederer, V. Gopalan, L. Q. Chen, D. G. Schlom, N. A. Spaldin, L. W. Martin, and R. Ramesh, Science **326**, 977 (2009).

[40] A. J. Hatt, N. A. Spaldin, and C. Ederer, Phys. Rev. B **81**, 054109 (2010).

[41] K. Miura, M. Kubota, M. Azuma, and H. Funakubo, Jpn. J. Appl. Phys. **49**, 09ME07 (2010).

[42] T. H. Cheng, K. L. Peng, C. Y. Ko, C. Y. Chen, H. S. Lan, Y. R. Wu, C. W. Liu, and H. H. Tseng, Appl. Phys. Lett. **96**, 211108 (2010).

[43] H. Morisaki, F. W. Ping, H. Ono, and K. Yazawa, J. Appl. Phys. **70**, 1869 (1991).

[44] Z. Luo, P. M. Vora, E. J. Mele, A. T. C. Johnson, and J. M. Kikkawa, Appl. Phys. Lett. **94**, 111909 (2009).

[45] P. Chen, N. J. Podraza, X. S. Xu, A. Melville, E. Vlahos, V. Gopalan, R. Ramesh, D. G. Schlom, and J. L. Musfeldt, Appl. Phys. Lett. **96**, 131907 (2010).

[46] M. Cai, J. Liu, G. Yang, Y. Cao, X. Tan, and X. Chen, J. Chem. Phys. **126**, 154708 (2007).

[47] X. Ming, X. Meng, Q. Xu, F. Du, Y. Wei, and G. Chen, RSC Adv. **4**, 64601 (2014).

[48] C. A. F. Vaz, J. Hoffman, A. B. Posadas, and C. H. Ahn, Appl. Phys. Lett. **94**, 022504 (2009).

[49] Z. Fang, I. V. Solovyev, and K. Terakura, Phys. Rev. Lett. **84**, 3169 (2000).

[50] W. Lu, W. D. Song, K. He, J. Chai, C. Sun, G. Chow, and J. Chen, J. Appl. Phys. **113**, 063901 (2013).

[51] E. O. Wollan and W. C. Koehler, Phys. Rev. **100**, 545 (1955).

[52] X. Ming, Q. Hu, F. Hu, F. Du, Y. Wei, and G. Chen, Comput. Mater. Sci. **119**, 33 (2016).

[53] Y. Nakamura, M. Kawai, M. Azuma, M. Kubota, M. Shimada, T. Aiba, and Y. Shimakawa, Jpn. J. Appl. Phys. **50**, 031505 (2011).

[54] X. Ming, X. Meng, F. Hu, C. Wang, Z. Huang, H. Fan, and G. Chen, J. Phys.: Condens. Matter **21**, 295902 (2009).

[55] U. Chowdhury, S. Goswami, D. Bhattacharya, A. Midya, and P. Mandal, Appl. Phys. Lett. **109**, 092902 (2016).

[56] A. G. Gavriliuk, V. V. Struzhkin, I. S. Lyubutin, S. G. Ovchinnikov, M. Y. Hu, and P. Chow, Phys. Rev. B **77**, 155112 (2008).

[57] T. Jia, H. Wu, G. Zhang, X. Zhang, Y. Guo, Z. Zeng, and H. Q. Lin, Phys. Rev. B **83**, 174433 (2011).